PROCEEDINGS OF SCIENCE

Understand and Search for New Aromatic Hydrocarbon Superconductors

Haiqing Lin[*,a] **Zhongbing Huang,**[a,b] **Guohua Zhong**[c] **and Xunwang Yan**[d]

[a] *Beijing Computational Science Research Center Beijing 100084, China*
[b] *Faculty of Physics and Electronic Technology, Hubei University Wuhan 430062, China*
[c] *Center for Photovoltaics and Solar Energy, Shenzhen Institutes of Advanced Technology, Chinese Academy of Sciences and The Chinese University of Hong Kong Shenzhen, 518055, China*
[c] *School of physics and electrical engineering, Anyang Normal University Henan 455000, China*
E-mail: haiqing0@csrc.ac.cn, huangzb@hubu.edu.cn, gh.zhong@siat.ac.cn, xwyan@csrc.ac.cn

In this talk, we present our systematic study on the aromatic hydrocarbon superconductors by using the first-principle calculation, exact diagonalization, and quantum Monte Carlo simulation techniques.

PACS: 74.20.Pq, 74.70.Kn, 74.70.Wz, 71.20.Rv, 71.15.Mb, 61.66.Hq

2013 International Workshop on Computational Science and Engineering,
14-17 October 2013
National Taiwan University, Taipei, Taiwan

[*] Speaker.

PoS(IWCSE 2013)009

1. Introduction

The superconductivity in organic materials is among the most fascinating phenomena and has been a subject of considerable interest in past decades. Since the first organic superconductor $(TMTSF)_2PF_6$ was synthesized in 1979 [1], several classes of organic superconductors have been discovered, such as the quasi-one-dimensional $(TMTSF)_2X$[2], two-dimensional (BEDT-TTF)$_2$X[3], K-intercalated C_{60}[4], and Ca-doped graphite [5], in which TMTSF is tetramethyltetraselenafulvalene ($C_{10}H_{12}Se_4$) and BEDT-TTF is bis(ethylenedithio)tetrathiafulvalene ($C_{10}H_8S_8$). The notable feature of organic superconductors is that there exits charge transfer between different two components in crystal and the carrier is delocalized over the the whole organic crystal by the π molecular orbits, which is closely related to their superconductivity.

Recently, the discovery of superconductivity in potassium intercalated picene ($C_{22}H_{14}$) [6] by R. Mitsuhashi *et al.* in 2010 has attracted growing interest in the condensed matter physics community. Subsequently, phenanthrene ($C_{14}H_{10}$)[7] and dibenzopentacene ($C_{30}H_{18}$)[8] were intercalated by potassium to synthesize new superconductors, which are composed of fused benzene rings and have similar molecular structure to picene. The three superconductors based on aromatic hydrocarbons provide a new platform to explore the relationship between crystal structure, electronic structure, magnetism and superconductivity. Besides alkali metal, alkaline earth and rare earth metal were adopted to intercalated into phenanthrene crystal to explore their superconductivity. In experiment, the high quality $Ba_{1.5}$phenanthrene[9] and La_1phenanthrene [10] superconductors were obtained with superconductive shielding fractions 40% and 46%, respectively.

The determination of crystal structure of metal doped picene, phenanthrene, and dibenzopentacene is an important prerequisite to understand the electronic behavior and superconducting mechanism in the aromatic superconductors. However, the detailed crystal structures of doped materials have not yet been reported in experiment, especially the metal atomic position, due to the degradation of sample in air and the limit of measurement techniques [11, 10]. In the first-principle simulations, the optimized lattice parameters for metal doped picene and phenanthrene have large discrepancies to the experimental measured values [12, 13, 14]. Meanwhile, the importance of electronic correlation and magnetism in the metal-doped aromatic solids was emphasized by several research groups [15, 16, 17, 18, 19]. On the other hand, the understanding of electronic states on a single molecule is useful for providing energy scale intermediate between the microscopic energetics at the level of carbon atom and the macroscopic scale of the molecular solids. The resulting many-body states form a basis for analyzing the low-energy physics at the length scale larger than the size of molecules.

In this paper, we summarize our recent works of performing a systematic study on the crystal and electronic structures of potassium and alkali-earth (Ba/Sr) metal doped phenanthrene by the first-principle calculations. To gain some insights on the effect of electronic correlations on the magnetic and pair binding properties of aromatic hydrocarbons, we study the electronic states on a single molecule with different benzene rings and structures. The paper is organized in the following order: The crystal and electronic structures of potassium and alkali-earth metal doped phenanthrene are first presented in Section II and III, respectively. Then the magnetic and pair binding properties of different aromatic molecules are investigated and presented in Section IV. Finally, the summary of our results is given. Some of results have been published elsewhere, e.g., Ref. [18]

Configuration	Source	a	b	c	β	V
	Expt. (Ref. 7)	8.430	6.134	9.417	98.18	482.0
	LDA (Ref. 14)	8.04	6.54	10.09	102.6	517.77
K2K1	This work	8.440	6.195	10.124	98.32	523.78
K3	This work	7.796	6.834	10.028	111.10	498.45

Table 1: Optimized lattice constants a,b,c (in Å), angle β between a and c axes, and volume V of a unit cell for the tripotassium-doped phenanthrene ($K_3C_{14}H_{10}$) with $P2_1$ symmetry, obtained with different approximations, compared with experiment and previous theoretical results. The interest is in two special configurations of K2K1 and K3 which are the nearest to experimental structure and the stablest case, respectively.

2. K-doped phenanthrene

2.1 Crystal structure of K_3phenanthrene

It is always important to obtain crystal structure of interested materials, which is also very challenging. Within the framework of the density functional theory (DFT), for the investigations of crystal structures, the Vienna *ab initio* simulation package (VASP)[20] was employed to carry out the full optimization calculations of the K-doped phenanthrene. Inner electrons were replaced by the projector augmented wave (PAW) method, while the monoelectronic valence electrons were expanded in plane waves with an cutoff energy of 600 eV. For the optimization, a conjugate-gradient algorithm was used to relax the ions into their instantaneous ground state. The Monkhorst-Pack k-point grids were generated according to the specified k-point separation 0.04 $Å^{-1}$. And the convergence thresholds were set as 10^{-5} eV in energy and 0.005 eV/Å in force. In the standard DFT, the local density approximation (LDA)[21] was adopted to describe the electronic exchange-correlation interactions.

With the difference of intercalated K atomic positions, dozens of configurations of $K_3C_{14}H_{10}$ have been tested starting from the experimental lattice constants.[7] From the search of structures, the initial positions of K atoms pay an key role during the optimization. Changing K atomic positions, we obtained some different configurations. Two optimal structures of $K_3C_{14}H_{10}$ were picked out from all of checked configurations. One is the geometrical structure nearest to experiment, called as K2K1 configuration shown in Fig. 1(b). The other one is the stablest configuration, called as K3 configuration shown in Fig. 1(c). As a comparison, we fixed the lattice constants at experimental values to relax the inner coordinates of all atoms, which is so-called experimental structure shown in Fig. 1(a). In fact, the experiment can present the lattice constants but can not determine the atomic positions. The optimized crystal parameters are summarized in Table I, compared with experimental and previous theoretical results. We find that the K2K1 is in agreement with experimental ones in crystal parameters, except for an expansion in the c direction which causes the small increase of cell volume. The predicted lattice constants of K2K1 configuration are $a = 8.440$, $b = 6.195$, and $c = 10.124$ in Å, and the angle $\beta = 98.32^\circ$ between a and c axes, respectively. Our LDA results are nearer the experiment than previous theoretical predictions[14]. For K3 configuration, its total energy is 0.28 eV/f.u. lower than that of K2K1. However, the optimized lattice constants are $a = 7.796$, $b = 6.834$, and $c = 10.028$ in Å, and the angle $\beta = 111.10^\circ$ between a

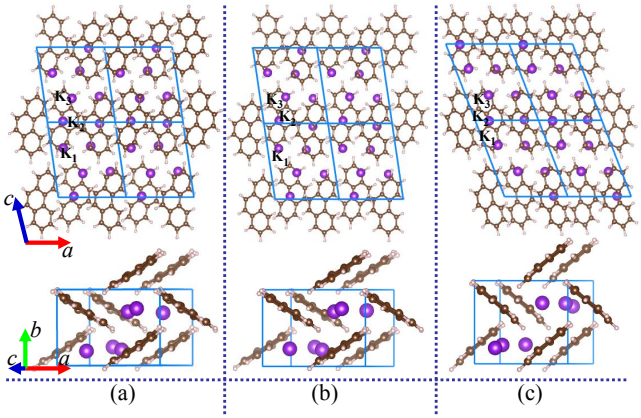

Figure 1: (Color online) Two special crystal configurations of tripotassium-doped phenanthrene comparing with the structure from the experimental lattice constants (a). K2K1 is a configuration of the nearest to experiment (b). K3 is the stablest case (c). Brown, grey and purple balls represent C, H, and K atoms, respectively. The top panels exhibit the $2 \times 1 \times 2$ supercells, while the bottom panels corresponding to one unit cell.

and c axes, respectively. There are the expansions in the b and c directions, an contraction in the a direction, and a big increase in the angle β, compared with experimental ones.

The K atoms are intercalated into the herringbone structure consisted of two phenanthrene molecular layer. The angle θ formed by two molecular layers in herringbone structure becomes smaller than that in undoped case. The geometrical configuration of K2K1 is similar to the previous theoretical prediction[14]. Looking at the geometry along the b direction, as the top panel shown in Fig. 1(b), two of three K atoms (K_2 and K_3) stay in the intralayer region (molecular layer) and respectively occupy a benzene ring near the C atom. The other K atom (K_1) removes into the interlayer region. It is just the cause of the K2K1 type. In the intralayer region, the atomic distances are 3.235 Å between K_2 and K_3 and 3.700 Å between K_1 and K_2, respectively. In the interlayer region, the atomic distance is 3.997 Å between K_1 and K_3. The expansion in the c direction in K2K1 configuration possibly results from the big distance of 3.997 Å between K_1 and K_3. In the intralayer region for K3 configuration, the atomic distances shorten to 3.172 Å between K_1 and K_2 and 3.179 Å between K_2 and K_3, respectively. In the interlayer region, the atomic distance increases to 4.045 Å between K_1 and K_3. Differing from K2K1, as shown in Fig. 1(c), all of three K atoms are in the intralayer region in K3 configuration due to the K_1 atom shifting toward phenanthrene molecule, which is also the cause of the K3 type. Additionally, the distance between two phenanthrene molecules along c direction becomes bigger in K3 than that in K2K1. It is one of causes of different geometries between these two configurations.

2.2 Electronic correlation effects in K_3phenanthrene

To observe the electronic correlations effects of K-doped phenanthrene, we have used the hybrid functionals method (HSE)[22, 23, 24]. In this method, the mixing coefficient ν presents the

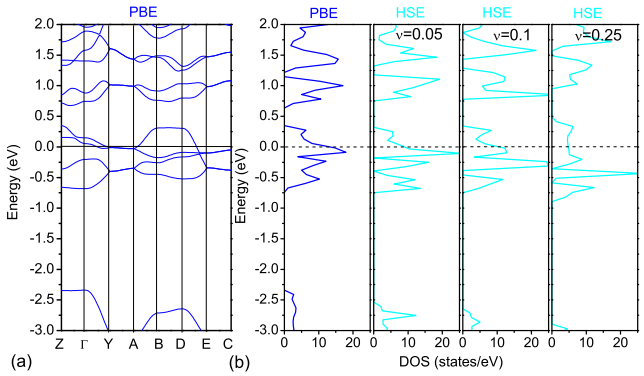

Figure 2: (Color online) Calculated band structure and total density of states (DOS) of $K_3C_{14}H_{10}$ at NM state. (a) Band structures based on the PBE level; (b) DOS based on PBE and HSE levels, respectively.

account of the Hartree-Fock exchange interaction and it is adjustable. The $\nu = 0$ means that the exchange-correlation functional returns to the level of the generalized gradient approximation (GGA) of Perdew-Burke-Ernzerhof (PBE) version[25]. Contrarily, the big ν values imply an increase of exchange-correlation effects. After K atoms doping into phenanthrene and adopting the crystal structure shown in Fig. 1(a), the total energy calculations suggest that $K_3C_{14}H_{10}$ is stabilized at nonmagnetic (NM) state. Figure 2(a) shows the band structures of $K_3C_{14}H_{10}$ based on PBE level. There are flat bands in the ranges of $Y-A$ and $B-D$ k-path directions, big dispersion in $Z-G$, $A-B$, and $D-E$ directions. Two bands cross the Fermi level which exhibits the visible metallic feature. K-3s electrons transport to C-2p orbitals and push the hybridization of C(2p)-C(2p) strengthen. The electronic states at the Fermi level mainly result from the C-2p electrons. However, the K-3d electrons contribute to the electronic states at Fermi level, hybridizing with the C-2p states. As a result, the bands are broadening, which will strongly weaken the electronic correlation. The electronic density of states (DOS) based on PBE and HSE levels shown in Fig. 2(b) prove the weak correlations in $K_3C_{14}H_{10}$. We notice that the $K_3C_{14}H_{10}$ keeps the metallic characteristics without the transition from metal to insulator (MIT), though the electronic exchange-correlation index ν reaches 0.25.

Another approach to better account for electron-electron interactions is to include the molecular Coulomb repulsion measured by the Hubbard parameter U_{eff}. It is therefore important to estimate the value of U_{eff}, which is essentially the energetic cost to doubly occupy a molecule including the screening effects of the other bands[26, 27, 28]. For doped phenanthrene, the U_{bare} can be obtained from the energies of the molecule charged with 2, 3, and 4 electrons as $U_{bare} = 2E(3) - E(2) - E(4)$. Such an estimate for an isolated molecule needs to be corrected ($E_{pol}(M)$) in order to include the screening effects in the solid. A first estimate can be obtained by considering the effect of the polarization of a charged molecule placed inside a cavity of a homogeneous dielectric medium characterized by a dielectric constant ε. Thus, $U_{eff} = U_{bare} - E_{pol}$. For $K_3C_{14}H_{10}$, the calculated U_{eff} is 0.67, 0.59, 0.52, 0.47, and 0.43 eV corresponding to the dielectric constants of 3.0, 3.5, 4.0, 4.5, and 5.0, respectively. The band width W is taken as the width of LUMO+1 band, 0.44 eV. Then the U_{eff}/W is in the range of $1.52 \sim 1.02$. The results also show the weak electronic

correlations effects in K-doped phenanthrene.

As a comparison, we also established the electronic correlation effects in K-doped picene. We found that the MIT occurred in the range of $0.15 < \nu < 0.2$. The calculated U_{eff}/W is in the range of $2.18 \sim 1.56$ corresponding to the dielectric constants from 3.0 to 5.0. The results indicate that the electronic correlation effects in K-doped picene is stronger than that in K-doped phenanthrene. Previous theoretical studies also proved the absence of metallicity in K-doped Picene[29].

3. Ba- and Sr-doped phenanthrene

3.1 crystal structure of $Ba_{1.5}$phenanthrene and $Sr_{1.5}$phenanthrene

In experiment, alkali earth metal barium and strontium are intercalated into phenanthrene to synthesize superconductor [9]. The ratio of metal atom and phenanthrene molecule is 1.5:1 to realize three electrons being transferred to per molecule. In our simulation, we construct the unit cell of $Ba_{1.5}$phenanthrene based on the pristine phenanthrene unit cell, namely we insert three Ba atoms in one unit cell of pristine phenanthrene to form the initial configuration for optimization. In phenanthrene crystal, the molecules are arranged in the herringbone manner to form one molecular monolayer, then the layers are stacked one by one along crystal axis *c* direction. The interstitial space among molecules in a layer can be considered a hole enclosed by four neighbor molecules.

For pristine phenanthrene, a unit cell includes two molecules and there are two holes in a unit cell averagely. To construct a unit cell of $Ba_{1.5}$phenanthrene, three Ba atoms are inserted into two holes belong to a unit cell of pristine phenanthrene. One case is that three Ba atoms enter in the same hole, and another case is that two Ba atoms occupy a hole and the third Ba atom occupy another hole, called them as $Ba_{1.5}$phenanthrene-I and $Ba_{1.5}$phenanthrene-II respectively. The optimized structure for $Ba_{1.5}$phenanthrene-I and $Ba_{1.5}$phenanthrene-II are shown in Fig. 3 and their lattice parameters are listed in Table.2.

Sr is another alkali earth metal element at the top of Ba in element periodicity. Sr atoms are also intercalated into phenanthrene to synthesize aromatic organic superconductor. Similar to the above Ba-doped phenanthrene, we perform the optimization of crystal structure for $Sr_{1.5}$phenanthrene. The lattice parameters for two structural phases are listed in Table.2. The optimized lattice parameters for Ba- or Sr-doped phenanthrene have a large discrepancy to the measured ones. The difficulty of crystal structure simulation also appeared in the previous studies on K-doped phenanthrene and K-doped picene [14, 13].

3.2 Electronic structure of $Ba_{1.5}$phenanthrene and $Sr_{1.5}$phenanthrene

The energy per unit cell of $Ba_{1.5}$phenanthrene-I is 0.33 eV lower than the value for $Ba_{1.5}$phenanthrene-II, so the structure phase of $Ba_{1.5}$phenanthrene-I is more stable. The energy band structure for $Ba_{1.5}$phenanthrene-I is presented in Fig. 4. On the whole, the bands around Fermi energy are flat and little dispersive, and the narrow band width lead to no overlap or very small overlap between two neighbor bands. There are two bands cross the Fermi level, which two bands are mainly from the next lowest unoccupied molecular orbital (LUMO+1 orbit). The energy gap from -2.5 $\sim$ -0.8 eV corresponds to the gap between the highest occupied molecular obital (HOMO) to LUMO. The band structure of $Sr_{1.5}$phenanthrene-I is similar to the $Ba_{1.5}$phenanthrene-I.

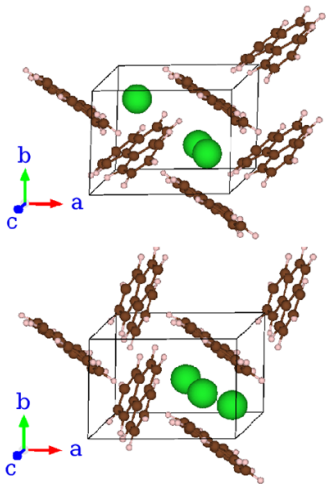

Figure 3: (Color online) Schematic structure of the unit cell of $A_{1.5}$phenanthrene-I and $A_{1.5}$phenanthrene-II (A=Ba or Sr). In the structure phase $A_{1.5}$phenanthrene-I, three metal atoms are distributed into two holes, while in $A_{1.5}$phenanthrene-I three metal atoms locate in a hole and another hole is not occupied. Green balls means the intercalated Ba or Sr atoms.

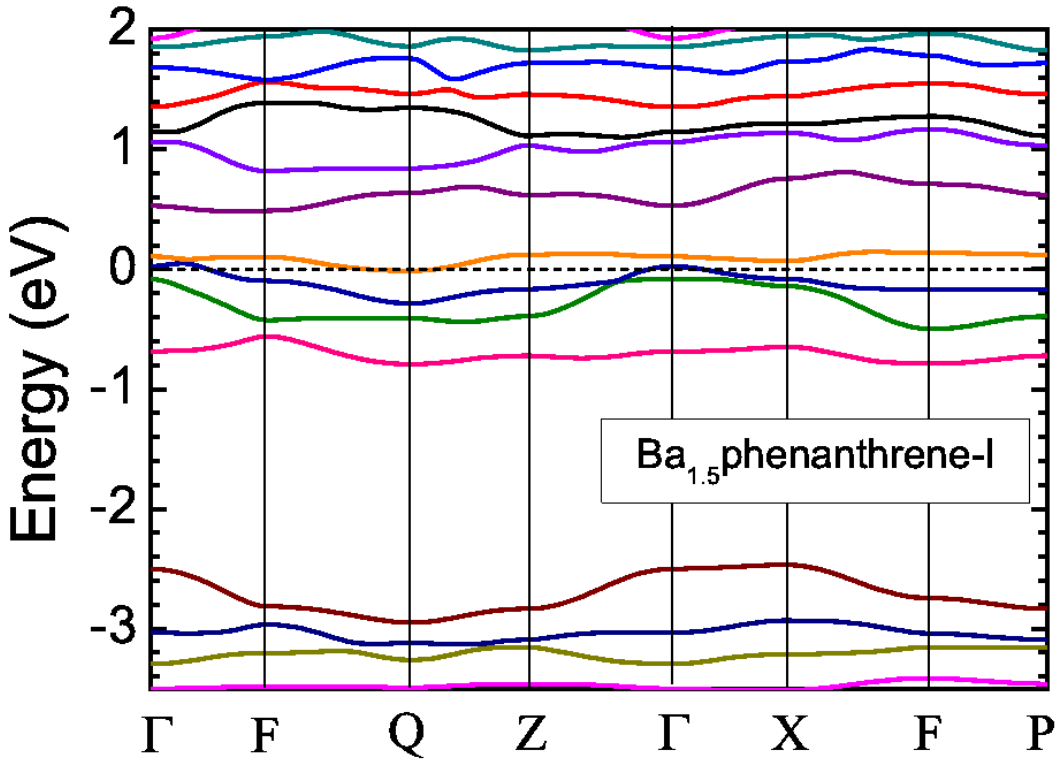

Figure 4: (Color online) Band structure of $Ba_{1.5}$phenanthrene-I.

	a	b	c	α	β	γ
$Ba_{1.5}$phenanthrene-I	8.03	6.04	8.85	89.88	101.37	89.08
$Ba_{1.5}$phenanthrene-II	8.41	5.83	8.84	90.18	100.33	88.88
Ba-doped Experiment[9]	8.48	6.18	9.50	90.0	97.49	90.0
$Sr_{1.5}$phenanthrene-I	7.87	5.95	8.75	89.63	1001.16	88.92
$Sr_{1.5}$phenanthrene-II	8.05	5.66	8.89	88.94	100.07	89.47
Sr-doped Experiment[9]	8.47	6.18	9.49	90.0	97.55	90.0

Table 2: The optimized lattice parameters for $Ba_{1.5}$phenanthrene-I, $Ba_{1.5}$phenanthrene-II and $Sr_{1.5}$phenanthrene-I, $Sr_{1.5}$phenanthrene-II, compared to the experimental values.

4. magnetic and pair binding properties on a single molecule

The minimal description of interacting p_π-electrons on a single molecule is given by the one-orbital Hubbard model which incorporates an on-site Coulomb repulsion besides a simple Huckel picture for the one-electron part [18]. The Hamiltonian reads,

$$H = -t \sum_{\langle ij\rangle,\sigma} (c^\dagger_{i\sigma} c_{j\sigma} + c^\dagger_{j\sigma} c_{i\sigma}) - \varepsilon \sum_i{}' n_i + U \sum_i n_{i\uparrow} n_{i\downarrow}, \tag{4.1}$$

The operators $c^\dagger_{i\sigma}$ and $c_{i\sigma}$ create and destroy a π-electron with spin σ at the ith carbon atom of a single molecule, respectively. $n_{i\sigma} = c^\dagger_{i\sigma} c_{i\sigma}$ is the number operator for an electron with spin σ at site i, and $n_i = n_{i\uparrow} + n_{i\downarrow}$. The sum $\langle ij\rangle$ is over nearest-neighbor (NN) carbon atoms, and the primed sum runs over the carbon sites without connecting to hydrogen atoms. Here, U denotes the on-site Coulomb interaction and ε the energy difference between carbon atoms with and without hydrogen bonds, which is due to different electron-negativity of carbon and hydrogen. Two accurate numerical methods, exact diagonalization (ED) and constrained-path Monte Carlo (CPMC), are employed to simulate the model Hamiltonian (4.1).

In our previous work [18], we have presented a detailed discussion on the magnetic and pair binding properties of phenanthrene, picene, and dibenzopentacene. In order to search for new aromatic hydrocarbon superconductors and understand the general physics of aromatic hydrocarbon molecules, here we extend our research to other molecules with different benzene rings and structures. Six typical molecules with 4, 5, and 6 benzene rings are shown in Fig. 5.

The spin phase diagram of different molecules is shown in Fig. 6 at $U = 1.5t$. Here, we present the results for the charged molecules with two added electrons. The total spin S of the ground state is obtained by comparing the energies in different spin sectors. The molecules not shown in Fig. 6 always lie in the lowest spin states ($S = 0$ for even N_e and $S = 1/2$ for odd N_e, with N_e denoting the total number of electrons). One can clearly see that for the two electrons added cases, the total spin S switches from 0 to 1 at a certain critical ε for all molecules shown in Fig. 5. This behavior is very similar to that of phenanthrene, picene, and dibenzopentacene, suggesting that there exists a strong magnetic instability for the molecules with a chain structure, when two electrons are added to the neutral molecules. Our results predict that the Curie-Weiss magnetic behavior can be observed in the metal-doped molecular crystal formed by the molecules shown in Fig. 5.

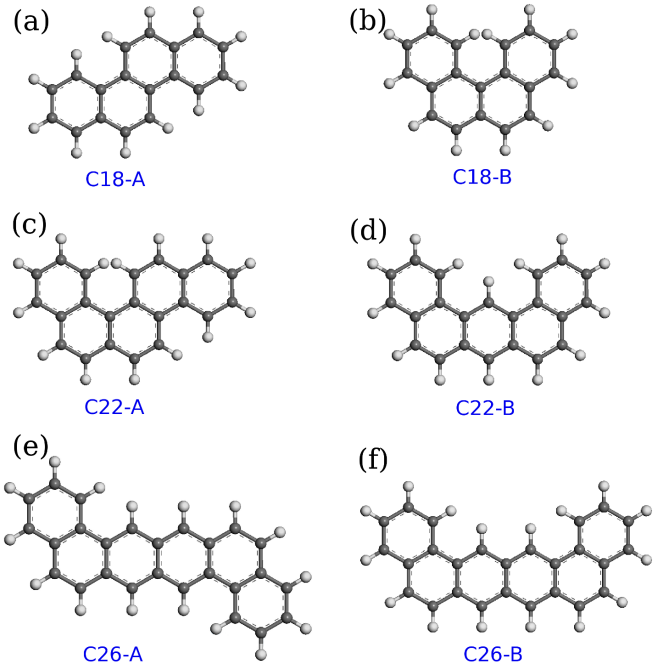

Figure 5: (Color online) Sketch of aromatic hydrocarbon molecules with (a) and 18 carbon atoms, (c) and (d) 22 carbon atoms, and (e) and (f) 26 carbon atoms.

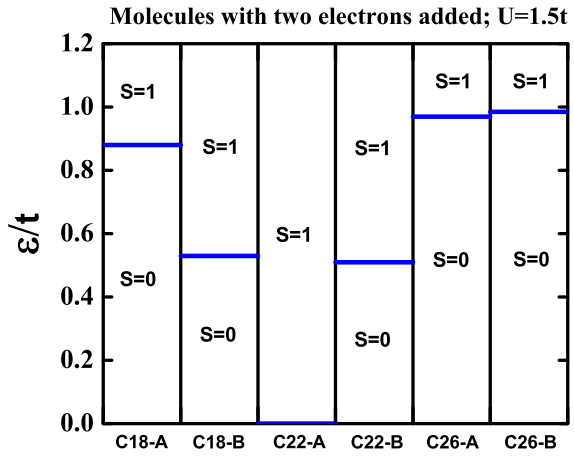

Figure 6: (Color online) Spin phase diagram for the hydrocarbon molecules with two electrons added as displayed in Fig. 5 at $U = 1.5t$. The total spin S of the ground state is shown for a combination of molecule structure and ε.

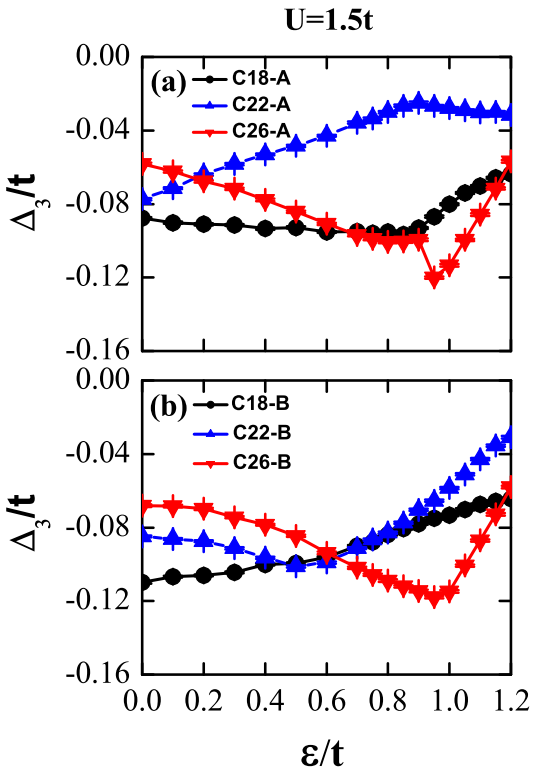

Figure 7: (Color online) Pair binding energy versus ε for the A-type (a) and B-type (b) molecules as shown in Fig. 5 at $U = 1.5t$. The molecular structure is indicated by the shape of symbol.

In Fig. 7, we show the pair binding energy Δ_3 as a function of ε for the molecules shown in Fig. 5. Here, $\Delta_3 = 2E_3 - E_2 - E_4$ with $E_{2,3,4}$ representing the ground state energy for the charged molecule having 2, 3, or 4 added electrons. In this notation, a positive Δ_3 implies that an effective attraction between added three electrons can be produced through a charge disproportionation process between the two molecules: $(3) + (3) \rightarrow (2) + (4)$, meaning that it is energetically favorable to have two molecules with 2 and 4 added electrons each rather than two molecules with 3 added electrons each. Fig. 7 shows that the pair binding energy is always negative in the whole parameter regime for all molecules considered. Therefore, it is expected electron correlation in the molecules is not enough for forming electron Cooper pairs, and electron-phonon interaction is necessary to be taken into account to produce attraction between added electrons.

Now we turn to discuss the pair binding property for some small molecules, which are displayed in Fig. 8. The corresponding pair binding energy Δ_3 is shown in Fig. 9. It is interesting to observe that Δ_3 for 9,10-dihydrophenanthrene, cis-stibene, and biphenyl is much less negative than that of phenanthrene in the parameter regime $\varepsilon < 0.8t$. This indicates that although electron correlation can not form electron Cooper pairs in these small molecules, the Coulomb pseudopotential between added electron is much weaker for 9,10-dihydrophenanthrene, cis-stibene, and biphenyl

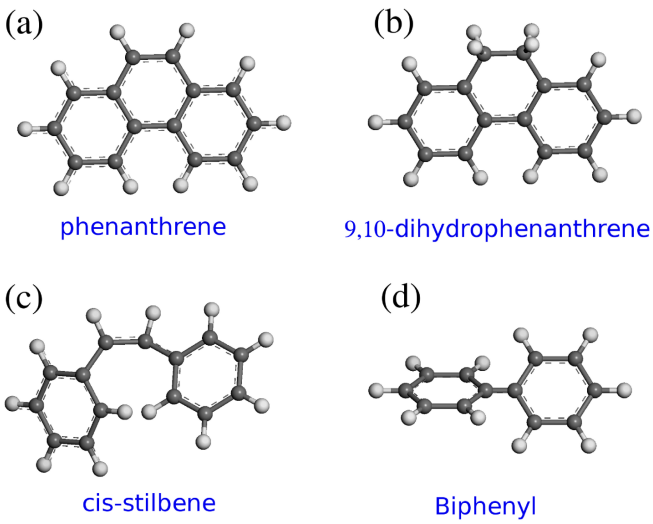

Figure 8: (Color online) Sketch of aromatic hydrocarbon molecules for (a) phenanthrene, (b) 9,10-digydrophenanthrene, (c) cis-stilbene, and (d) biphenyl.

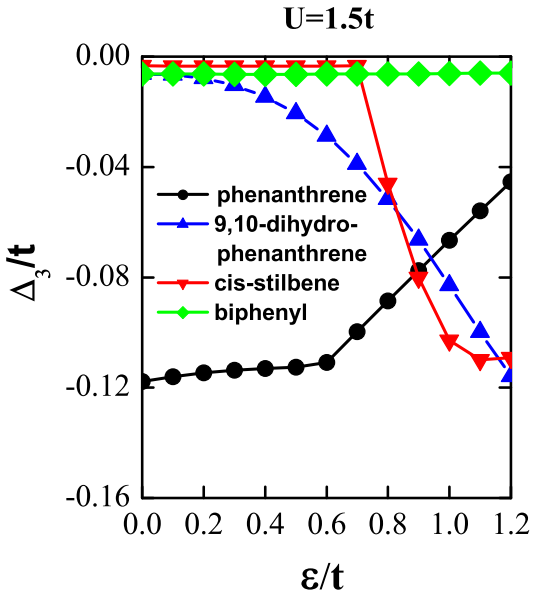

Figure 9: (Color online) Pair binding energy versus ε for the molecules as shown in Fig. 8 at $U = 1.5t$. The molecular structure is indicated by the shape of symbol.

than for phenanthrene. Assuming the electron-phonon coupling strength is similar in the four molecules, higher superconducting transition temperature T_c could be realized in the metal-doped molecular crystals formed by the former three molecules.

5. Conclusions

By carrying extensive numerical studies, we obtained likely crystal structures of undoped and doped aromatic hydrocarbon superconductors, and gain understandings on its magnetic and superconducting properties. Needless to say, main issues remain to settle. For example, the correct crystal structure when doped, the role of electron-electron and electron-phonon correlations, the driving force for the superconductivity, etc. Much more efforts in both theory and experiment are called for.

6. Acknowledgments

This work was supported by MOST 2011CB922200, the Natural Science Foundation of China under Grants Nos. 91221103, 11174072, U1204108, and 11274335.

References

[1] K. Bechgaard, C. S. Jacobsen, K. Mortensen, H. J. Pedersen, and N. Thorup, *The properties of five highly conducting salts: (TMTSF)$_2$X, X = PF_6-, AsF_6-, SbF_6-, BF_4- and NO_3-, derived from tetramethyltetraselenafulvalene (TMTSF)*, *Solid State Communications*, **33** (Mar., 1980) 1119.

[2] T. Ishiguro, K. Yamaji, and G. Saito, *Organic Superconductors*, (Berlin, Heidelberg; Springer Berlin Heidelberg, **ISBN**:978-3-540-63025-8) (1998).

[3] H. Urayama, H. Yamochi, G. Saito, K. Nozawa, T. Sugano, M. Kinoshita, S. Sato, K. Oshima, A. Kawamoto, and J. Tanaka, *A new ambient pressure organic superconductor based on BEDT-TTF with Tc higher than 10K (T_c = 10.4 K)*, *Chem. Lett.*, **17** (1988) 55.

[4] A. F. Hebard, M. J. Rosseinsky, R. C. Haddon, D. W. Murphy, S. H. Glarum, T. T. M. Palstra, A. P. Ramirez, and A. R. Kortan, *Superconductivity at 18 K in potassium-doped C60*, *Nature* **350** (Apr., 1991) 6319.

[5] N. Emery, C. Hérold, M. D'Astuto, V. Garcia, Ch. Bellin, J. Marêché, P. Lagrange, and G. Loupias, *Superconductivity of Bulk CaC_6*, *Phys. Rev. Lett.* **95** (Aug., 2005) 087003.

[6] R. Mitsuhashi, Y. Suzuki, Y. Yamanari, H. Mitamura, T. Kambe, N. Ikeda, H. Okamoto, A. Fujiwara, M. Yamaji, N. Kawasaki, Y. Maniwa, and Y. Kubozono, *Superconductivity in alkali-metal-doped picene*, *Nature* (London) **464** (Mar.,2010) 76.

[7] X. F. Wang, R. H. Liu, Z. Gui, Y. L. Xie, Y. J. Yan, J. J. Ying, X. G. Luo, and X. H. Chen, *Superconductivity at 5 K in alkali-metal-doped phenanthrene*, *Nat. Commun.* **2** (Jan., 2011) 507.

[8] M. Q. Xue, T. B. Cao, D. M. Wang, Y. Wu, H. X. Yang, X. L. Dong, J. B. He, F. W. Li, and G. F. Chen, *Superconductivity above 30 K in alkali-metal-doped hydrocarbon*, *Sci. Rep.* **2** (Jan., 2012) 389.

[9] X. F. Wang, Y. J. Yan, Z. Gui, R. H. Liu, J. J. Ying, X. G. Luo, and X. H. Chen, *Superconductivity in $A_{1.5}$phenanthrene (A =Sr,Ba)*, *Phys. Rev. B* **84** (Dec., 2011) 214523.

[10] X. F. Wang, X. G. Luo, J. J. Ying, Z. J. Xiang, S. L. Zhang, R. R. Zhang, Y. H. Zhang, Y. J. Yan, A. F. Wang, P. Cheng, G. J. Ye, and X. H. Chen, *Enhanced superconductivity by rare-earth metal doping in phenanthrene*, *J. Phys. Condens. Matter* **24** (Aug., 2012) 345701.

[11] Y. Kasahara, T. Yuki, and I. Yoshihiro, *Bulk superconductivity and fully gapped superconducting state in Ba-doped phenanthrene*, *Phys. Rev. B* **85** (Jun., 2012) 214520.

[12] T. Kosugi, T. Miyake, S. Ishibashi, R. Arita, and H. Aoki, Hideo, *First-principles structural optimization and electronic structure of the superconductor picene for various potassium doping levels*, *Phys. Rev. B* **84** (Dec., 2011) 214506.

[13] P. L. de Andres, A. Guijarro, and J. A. Vergés, *Crystal structure and electronic states of tripotassium picene*, *Phys. Rev. B* **83** (Jun., 2011) 245113.

[14] P. L. de Andres, A. Guijarro, and J. A. Vergés, *Ab initio electronic and geometrical structures of tripotassium-intercalated phenanthrene*, *Phys. Rev. B* **84** (Oct., 2011) 144501.

[15] M. Kim and B. I. Min, *Density functional calculations of electronic structure and magnetic properties of the hydrocarbon K_{3}picene superconductor near the metal-insulator transition*, *Phys. Rev. B* **83** (Jun., 2011) 214510.

[16] G. Giovannetti and M. Capone, *Electronic correlation effects in superconducting picene from ab initio calculations*, *Phys. Rev. B* **83** (Apr., 2011) 134508.

[17] M. Kim, H. C. Choi, J. H. Shim, and B. I. Min, *Correlated Electronic Structures and the Phase Diagram of Hydrocarbon-based Superconductors*, *New J. Phys.* **15** (Apr., 2013) 113030.

[18] Z. B. Huang, C. Zhang, and H. Q. Lin, *Magnetic instability and pair binding in aromatic hydrocarbon superconductors*, *Sci. Rep.* **2** (Jan., 2012) 922.

[19] J. A. Vergés, P. L. de Andres, E. San-Fabián, G. Chiappe, G. E. Louis, and A. Guijarro, *Spin alignment of extra electrons in K-phenanthrene clusters taken from the crystalline tripotassium-intercalated phenanthrene structure*, *Phys. Rev. B* **85** (Apr., 2012) 165102.

[20] G. Kresse and J. Furthmuller, *Efficiency of ab-initio total energy calculations for metals and semiconductors using a plane-wave basis set*, *Comput. Mater. Sci.* **6** (Jul., 1996) 15.

[21] J. P. Perdew and Y. Wang, *Accurate and simple analytic representation of the electron-gas correlation energy*, *Phys. Rev. B* **45** (Jun,. 1992) 13244.

[22] J. Heyd, G. E. Scuseria, and M. Ernzerhof, *Hybrid functionals based on a screened Coulomb potential*, *J. Chem. Phys.* **118** (Apr., 2003) 8207.

[23] J. Heyd and G. E. Scuseria, *Efficient hybrid density functional calculations in solids: assessment of the Heyd-Scuseria-Ernzerhof screened Coulomb hybrid functional*, *J. Chem. Phys.* **121** (Jul., 2004) 1187.

[24] J. Heyd, G. E. Scuseria, and M. Ernzerhof, *Erratum: qřHybrid functionals based on a screened Coulomb potentialąś [J. Chem. Phys. 118 (Feb., 2003) 8207]*, *J. Chem. Phys.* **124** (Jun., 2006) 219906.

[25] J. P. Perdew, K. Burke, and M. Ernzerhof, *Generalized Gradient Approximation Made Simple*, *Phys. Rev. Lett.* **77** (Oct., 1996) 3865.

[26] M. F. Craciun, G. Giovannetti, S. Rogge, G. Brocks, A. F. Morpurgo, and J. van den Brink, *Evidence for the formation of a Mott state in potassium-intercalated pentacene*, *Phys. Rev. B* **79** (Mar., 2009) 125116.

[27] G. Giovannetti, G. Brocks, and J. van den Brink, *Ab initio electronic structure and correlations in pristine and potassium-doped molecular crystals of copper phthalocyanine*, *Phys. Rev. B* **77** (Jan., 2008) 035133.

[28] G. Brocks, J. van den Brink, and A. F. Morpurgo, *Electronic Correlations in Oligo-acene and -Thiopene Organic Molecular Crystals*, *Phys. Rev. Lett.* **93** (Sep., 2004) 146405.

[29] A. Ruff, M. Sing, R. Claessen, H. Lee, M. Tomić, H. O. Jeschke, and R. Valentí, *Absence of Metallicity in K-doped Picene: Importance of Electronic Correlations*, *Phys. Rev. Lett.* **110** (May, 2013) 216403.